Pergamon

Int. J. Solids Structures Vol. 32, No. 16, pp. 2393–2418, 1995

0020–7683/95 $9.50 + .00

0020–7683(94)00187–1

ENHANCED ELASTIC–PLASTIC LINE-SPRING FINITE ELEMENT

HYUNGYIL LEE and DAVID M. PARKS
Department of Mechanical Engineering, Massachusetts Institute of Technology, Cambridge, MA 02139, U.S.A.

(*Received* 21 *September* 1993; *in revised form* 28 *July* 1994)

Abstract—The elastic–plastic line-spring finite element of Parks and White (1982), as implemented in the ABAQUS finite element code (1988b), is modified in several ways for a better evaluation of crack-tip deformation parameters such as K_I, J, crack-tip opening displacement and crack-tip stress triaxiality, the last of which is inferred or measured by the so-called T-stress and Q-stress parameters. An effective crack length formulation is introduced to capture the nonlinearity due to contained plane strain crack-tip plastic deformation, the size and orientation of which are known to be sensitive to the sign and magnitude (relative to yield strength) of the T-stress. More accurate yield surfaces, obtained from finite element limit analyses of plane strain single-edge cracked specimens, are employed to more sharply define the behavior of the line-spring model in the fully plastic region. More accurate relationships between incremental plastic crack-tip opening displacement and incremental load point displacement/rotation are also incorporated into the model for shallow crack configurations under fully plastic loading. The modified line-spring model is then applied to surface cracked plate problems having a wide range of crack-tip constraints, and the feasibility of implementing J–$T(Q)$ based two-parameter characterizations of elastic–plastic crack front fields via simplified line-spring elements is examined.

1. INTRODUCTION

The analysis of a part-through surface crack in a plate or a shell is an important problem in engineering fracture mechanics. The geometry of the surface crack leads to an intrinsically three-dimensional (3-D) problem having a strong interaction between the crack front field and the bounding surface of the body. Due to the difficulties in constructing closed-form solutions, the majority of existing solutions rely heavily on numerical techniques. Although 3-D finite element methods are available for the general elastic–plastic problems of the surface crack, the enormous computer storage, extensive computational times, and large amounts of data preparation and reduction associated with the geometric and parametric complexities of the surface crack make the routine application of 3-D FEM currently impractical. However, many of these problems can be solved with a simplified model called the line-spring.

The line-spring model was introduced by Rice and Levy (1972) to effectively calculate the stress intensity factors (K_I) of part-through surface cracks in plate or shell structures. The evaluation of the elastic T-stress in surface cracked plates using the line-spring finite element, by Wang and Parks (1992), illustrated another important application of the model to the study of two-parameter crack-tip characterization. The virtue of the line-spring model is that it reduces complex 3-D problems to tractable "two-dimensional" plate/shell problems.

The model was incorporated into singular integral equation formulations of isotropic elastic plate or thin shell theory (Delale and Erdogan, 1981; Parks, 1981). For problems in which structural models more general than thin elastic shell theory are required, the linear elastic line-spring was implemented in a general finite element program (Parks *et al.*, 1981). The numerical results for K_I from these elastic analyses were within a few percent of accepted solutions along most of the surface crack front. The nonlinear elastic line-spring model based on the deformation theory of plasticity (Kumar and German, 1985; Miyoshi *et al.*, 1986; Shawki *et al.*, 1989) would be most appropriate for proportional loading cases.

Parks (1981) noted, however, that the evolution of nonuniform inelastic response in line-spring models of surface cracked plates often leads to rather nonproportional force/moment trajectories. Moreover, the line-spring model is a promising potential tool for assessing problems of substantial through-thickness penetration, e.g. the leak before break problem (Lee and Parks, 1994), because it does not require any remeshing for simulation of crack growth in the thickness direction. Consequently, an approach based on the incremental theory of plasticity is likely to be more appropriate. Parks and White (1982) presented an elastic–plastic model of the line-spring finite element using the incremental theory of plasticity. Their model, as implemented in the ABAQUS finite element code (1988b), is very accurate in the linear elastic region and generally gives a good estimate of non-hardening limiting loads. Nonetheless, the accuracy of their line-spring model could be improved in the elastic–plastic transition region and in the fully plastic hardening region.

Here, in a straightforward modification of the line-spring model of Parks and White (1982), we introduce a new effective crack length formulation (Hauf *et al.*, 1994) to capture the deviation of load vs displacement curve from linearity in the contained yielding region, thereby providing a smooth and realistic transition between linear elastic and fully plastic regions. Model performance in the fully plastic region is enhanced by adopting accurate tabulated yield surfaces of plane strain single-edge cracked (SEC) specimens (Lee and Parks, 1993), and by calibrating the model's strain hardening factor on a more realistic stress–strain curve. Finally, we compare the line-spring solutions with 3-D finite element solutions, and investigate the feasibility of implementing J–$T(Q)$ based two-parameter characterization of elastic–plastic crack front fields (Betegón and Hancock, 1991; O'Dowd and Shih, 1991, 1992; Wang, 1993) via simple line-spring modeling.

2. THE LINE-SPRING MODEL

Additional compliance is introduced into a plate or shell structure by the presence of a part-through surface crack. The main feature of the line-spring model is that this additional compliance is accounted for by a through-crack of length $2c$ in the shell, with a generalized foundation connecting the two sides of the model through-crack. Consider a part-through surface crack of total length $2c$ in a shell of thickness t, as illustrated schematically in Fig. 1. The coordinate x measures the distance from the center line ($x = 0$) of the surface crack.

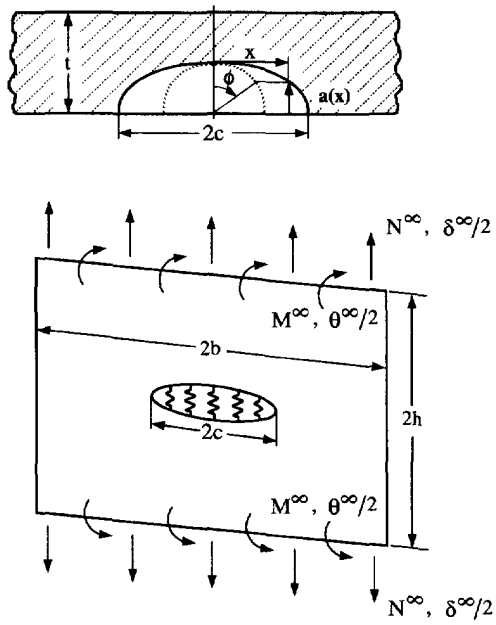

Fig. 1. Cross section of a part-through surface crack with a length $2c$ and varying depth $a(x)$ in a shell of thickness t (above). Schematic illustration of line-spring model which converts the part-through surface crack to the through-crack with a generalized foundation (below).

The local depth of the surface crack is $a(x)$, where $0 \leqslant a(x) \leqslant t$ for $|x| \leqslant c$. In symmetrically loaded structures, the generalized shell resultants transmitted by the foundation are a membrane force $N(x)$ and a bending moment $M(x)$ per unit length. Kinematic variables work-conjugate to the local force and moment are relative separation and rotation $[\delta(x), \theta(x)]$ of the model through-crack. The foundation in Fig. 1 has a compliance which varies according to the local crack depth $a(x)$ of the surface crack. The surface crack reduces to the plane strain SEC specimen if $2c \gg t$, and $a(x)$ is essentially constant. With this limiting case as a motivation, the compliance of the foundation at x is taken from the additional *cracked* compliance of a plane strain SEC specimen having the same thickness t and crack depth $a(x)$ (Rice, 1972a; Rice and Levy, 1972). Because of this feature, the line-spring model is generally more accurate for surface cracks having larger crack length to shell thickness ratios $(2c/t)$ and gradually changing crack depth profiles $a(x)$.

The introduction of the additional compliance, lumped on the foundation along the discontinuity line of the cut in a shell, converts the 3-D surface crack problem to a generalized 2-D boundary value problem. When the combined shell and foundation model subject to remote loading is solved, the incremental generalized displacements and forces at the foundation are recovered. Finally, the crack front deformation parameter at position x [as measured by $K_I(x)$, $J(x)$ and crack-tip opening displacement, CTOD(x), etc.] is estimated as the same value which would occur in the plane strain SEC specimen of thickness t and crack depth $a(x)$ subject to the combined load histories $[N(x), M(x)]$.

2.1. *Effective crack length formulation*

Renamed as $Q_1 = N$, $Q_2 = M$; $q_1 = \delta$, $q_2 = \theta$, the generalized displacements and forces are connected in the linear elastic region by the elastic compliance matrix P_{ij}:

$$q_i = P_{ij}(a, t)Q_j \tag{1}$$

where the summation convention (from 1 to 2) on repeated indices is adopted. The elastic compliance matrix P_{ij} is determined from the mode I stress intensity factor calibrations of the SEC specimen using the energy/compliance relation (Rice, 1972b)

$$P_{ij} = \frac{2}{H}\int_0^a F_i(\bar{a}, t)F_j(\bar{a}, t)\,\mathrm{d}\bar{a} \tag{2}$$

where $H = E/(1-\nu^2)$, E is Young's modulus and ν is Poisson's ratio. The functions $F_i(a, t)$ $(i = 1,2)$ contain the K_I-calibrations of the SEC specimen subject to tension (F_1) and bending (F_2); that is, $K_I(Q_i; a, t) = F_i(a, t)Q_i$ by superposition. These calibration functions are readily obtained from the handbook, for example, of Tada *et al.* (1985).

Rice (1972a) noted that the transition from linear elastic to fully plastic conditions in the line-spring model might be smoothed by use of a plastically adjusted *effective crack length* a_{eff}, and Parks (1981) made limited use of such a construct. The line-spring of Parks and White (1982), herein denoted the PW line-spring, did not include such smoothing. Here, we introduce the effective crack length as a simple way to account for load/displacement nonlinearity within the initial yield surface, $\Phi(Q_i; a, t; \tau_y) < 0$. Here Φ is a yield function in the generalized force space and τ_y is the yield strength in shear, which is related to the tensile yield strength by $\tau_y = \sigma_y/\sqrt{3}$ according to a von Mises yield criterion. A work hardened surface $\Phi(Q_i; a, t; \tau_o) = 0$ based on the ligament-average shear flow strength $\tau_o(\geqslant \tau_y)$ will be called the "yield surface", while the surface $\Phi(Q_i; a, t; \tau_y) = 0$ based on τ_y is termed the "initial" yield surface. Although the yield function $\Phi = 0$ is used to characterize the fully plastic state, in general, it does not describe the nonlinearity occurring at $\Phi < 0$ due to contained yielding.

Local crack-tip plasticity increases the remote displacements beyond their elastically calculated values, so that the effective compliance exceeds that of the purely elastic case. In other words, when observed in the remote elastic field, the crack appears longer than its physical size due to the occurrence of crack-tip plasticity (Irwin, 1958). The effective crack

length is generally taken as the sum of the physical crack length a and a correction proportional to the crack-tip plastic zone size. Crack-tip plastic zone size is more sensitive to the sign and magnitude of T-stress than are other crack-tip parameters such as CTOD (Rice, 1974). The stress field near the crack-tip in a linear elastic body under mode I loading is described by the Williams (1957) eigen-expansion, the first two terms of which are

$$\sigma_{ij}(r,\theta) = \frac{K_I}{\sqrt{2\pi r}} f_{ij}(\theta) + T\delta_{1i}\delta_{1j}. \tag{3}$$

Here $x_i (i = 1,2)$ are local Cartesian coordinates centered at the crack-tip, and the x_2-direction is normal to the crack faces. Cylindrical coordinates (r,θ) centered at the crack-tip are $r = \sqrt{x_1^2 + x_2^2}$ and $\theta = \tan^{-1}(x_2/x_1)$, and the functions $f_{ij}(\theta)$ provide the angular variation of the singular part of the respective stress components. (Through the context, the crack-tip polar coordinate "θ" is distinguished from the far field rotation "θ" of the SEC specimen.) The T-stress is a tensile or compressive stress acting parallel to the cracked plane, and δ_{ij} is the Kronecker delta.

With the effect of T-stress on plastic zone size included, the effective crack length can be expressed in the form

$$a_{\text{eff}} = a + \beta\rho(\tau)\left[\frac{K_I(\hat{a}_{\text{eff}},t)}{\sigma_y}\right]^2 \tag{4}$$

where a is the actual crack length, σ_y is the tensile yield strength, and β is a dimensionless parameter depending on the correction model and the strain hardening exponent of the material (Hauf *et al.*, 1994). The dimensionless function $\rho(\tau)$, with argument $\tau \equiv T/\sigma_y$, is taken from Wang's (1991) work. For a power law hardening material with hardening exponent $n = 10$, Wang (1991) obtained the plastic zone size at various values of τ by remotely applying the stress fields defined by (3) to a large semi-circular domain. In Fig. 2, the ratio of the maximum plastic zone radius at any given τ to the maximum plastic zone radius at small scale yielding, $R(\tau) \equiv r_p^{\max}|_\tau / r_p^{\text{SSY}}$, is plotted on logarithmic scale against τ, where $r_p^{\text{SSY}} \equiv r_p^{\max}|_{\tau=0}$. Wang's circled data can be fitted with a fourth order polynomial as

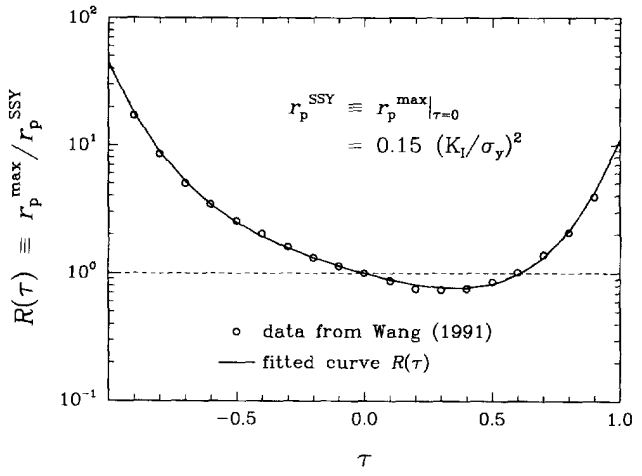

Fig. 2. Ratio of the maximum plastic zone radius at any given τ to the maximum plastic zone radius at $\tau = 0$, $R(\tau) \equiv r_p^{\max}|_\tau / r_p^{\max}|_{\tau=0}$, plotted on logarithmic scale against τ. The ratio $0.15\,R(\tau)$ is taken as $\rho(\tau)$ in eqn (4).

$$\log_{10} R(\tau) \equiv \log_{10}\left(\frac{r_p^{\max}|_\tau}{r_p^{SSY}}\right) \doteq c_1\tau + c_2\tau^2 + c_3\tau^3 + c_4\tau^4 \tag{5}$$

where fitting coefficients $(c_1, c_2, c_3, c_4) = (-0.539, 0.375, 0.236, 0.974)$. With reference to (4), we simply took $\rho(\tau) = 0.15\ R(\tau)$. Note that since $r_p^{SSY} \simeq 0.15(K_I/\sigma_y)^2|_{\tau=0}$, K_I in (4) is calibrated with $\hat{a}_{eff}$ corresponding to the effective crack length evaluated at $\tau = 0$, that is, the standard effective crack length,

$$\hat{a}_{eff} = a + 0.15\beta\left[\frac{K_I(\hat{a}_{eff}, t)}{\sigma_y}\right]^2. \tag{6}$$

Because a_{eff} plays its role in the contained yielding region ($\Phi < 0$) prior to gross work hardening in the ligament, the tensile yield strength, rather than a work hardened flow strength, is used in the correction.

In the standard formulation of plastically corrected effective crack length, K_I itself depends implicitly on the current loads and the effective crack length as

$$K_I(a_{eff}, t) = F_i(a_{eff}, t)Q_i. \tag{7}$$

The corresponding effective value of the "elastic" J-integral is

$$J = \frac{K_I^2}{H} = \frac{[F_i(a_{eff}, t)Q_i][F_j(a_{eff}, t)Q_j]}{H}. \tag{8}$$

Like K_I, T-stress is a function of geometry and loading conditions, and is proportional to the applied load (Larsson and Carlsson, 1973). Analogously to the stress intensity factor formulation, an effective value of T-stress in the elastic–plastic SEC specimen can be estimated as

$$T = t_i(a_{eff}/t)\hat{Q}_i. \tag{9}$$

Here $t_i(a_{eff}/t)$ are T-calibrators for the SEC specimen in tension and bending, and generalized load measures $\hat{Q}_1 = Q_1/t$, $\hat{Q}_2 = 6Q_2/t^2$ have dimensions of stress. Sham (1991) tabulated the t_i-functions of SEC specimens for essentially the entire range of a/t ($0.1 \leqslant a/t \leqslant 0.9$) using second order weight functions. When $a/t \to 0$, both t_i-functions are estimated as $t_i \doteq -0.51$ from a finite element result (Harlin and Willis, 1988). Supplementing this limiting value to Sham's data, for the range of $0 \leqslant a/t \leqslant 0.8$, we fitted tabulated data with a fourth order polynomial function such that $t_i = \sum_{k=0}^{k=4} a_k(a/t)^k$, where $(a_k, k = 0,4)$ are $(-0.501, -1.842, 14.48, -45.03, 47.42)$ for t_1 in tension, and $(-0.505, 0.906, 3.637, -10.73, 14.08)$ for t_2 in bending. Note that as $a/t \to 0$, $t_i \to a_0$, and the fitted values of $a_0 = -0.501$ (tension) and -0.505 (bending) are in good agreement with the results of Harlin and Willis (1988). These fourth order polynomial functions are used for T-stress calibrations in our line-spring model.

The total complementary strain energy of a cracked configuration, Ω_t, can be considered as the sum of that absent from the crack (Ω_{nc}) and that due to the crack (Ω_c) (Rice *et al.*, 1973); $\Omega_t = \Omega_{nc} + \Omega_c$. With this decomposition, Hauf *et al.* (1994) derived an expression for the cracked displacements in terms of the effective crack length as summarized below. The additional cracked displacements of q_i of the load point are given as

$$q_i = \frac{\partial\Omega_c}{\partial Q_i}. \tag{10}$$

Further, by the definition of the J-integral,

$$J \equiv \frac{\partial \Omega_c}{\partial a} \Leftrightarrow \Omega_c = \int_0^a J \, d\bar{a}. \tag{11}$$

Introducing (8) into (11), and combining (10) and (11) provides

$$q_i = \frac{2}{H} \int_0^a K_I(a_{eff}, t) \frac{\partial K_I(a_{eff}, t)}{\partial Q_i} d\bar{a} \tag{12}$$

where it is understood that $a_{eff}(\bar{a}, t, Q_i)$ from (4)–(9) depends functionally on the integration variable $\bar{a}$ in (12). In practice, the integrals (12) are evaluated numerically. Thus, the relation between cracked displacements and generalized forces in the contained yielding region is obtained in an energetically consistent form, leading to a symmetric Jacobian $\partial Q_i/\partial q_j$ as summarized in Section A1 of the Appendix.

2.2. *Yield surfaces*

The construction materials used for pressure vessels and piping are often so ductile under operating conditions that all or part of the ligament can undergo fully plastic deformation prior to fracture initiation. Hence it is of practical significance to assure accuracy of the line-spring model in the fully plastic regime. The line-spring model employs a convex yield surface $\Phi(Q_i; a, t; \tau_o) = 0$ in the generalized force space. An explicit approximate form for the yield surface under conditions of predominant tension was provided by Rice (1972a) and by Kim *et al.* (1994a), and another explicit form in a load state of predominant bending was discussed by Shiratori and Miyoshi (1980) and by White *et al.* (1983).

Applying the upper bound theorem to a kinematically admissible flow field consisting of a single circular arc, Rice (1972a) constructed an upper bound yield surface graphically. Then he approximated the upper bound yield surface with the following explicit elliptical equation

$$\Phi_R = \left[\frac{(N/2\tau_o l) - 0.3}{0.7}\right]^2 + 9\left[\frac{M + Na/2}{2\tau_o l^2}\right]^2 - 1 = 0 \tag{13}$$

where τ_o is the flow strength in shear, a is the crack length and l is the remaining ligament ($t = a + l$). This elliptical equation was used in the PW line-spring model. When a positive bending moment, superposed with an axial force of a magnitude less than $0.55 \cdot (2\tau_o l)$, is applied to the SEC specimen, the Green and Hundy (GH) field (1956) for pure bending can be modified to produce a slip-line field for the combined load state. Adding a compressive force region to the GH field, White *et al.* (1983) derived the following yield surface:

$$\Phi_{MGH} = \frac{M}{\tau_o l^2} - \frac{N}{2\tau_o l}(0.26 - a/l) + 0.37\left(\frac{N}{2\tau_o l}\right)^2 - 0.63 = 0. \tag{14}$$

The exact yield surface of the plane strain uncracked strip of thickness t in rigid/plastic material, subject to combined tension and bending, is given by Prager (1959):

$$\Phi_U = \frac{2|M|}{\tau_o t^2} + \left(\frac{N}{2\tau_o t}\right)^2 - 1 = 0. \tag{15}$$

If the thickness t in (15) is replaced by the ligament l of the SEC specimen, and the moment M in (15) is re-interpreted as the moment about mid-ligament rather than mid-specimen, this yield surface becomes a lower bound yield surface for the SEC specimen.

The yield surfaces defined by eqns (13) and (14) are for cracks sufficiently deep that yielding is confined to the ligament. As studied by Green (1956), Ewing (1968) and Matsoukas *et al.* (1986), the slip-line field of the shallow crack configuration in predominant bending extends to the front surface. Good detection techniques allow shallow cracks to be the ones most encountered in engineering practice. In accidental overloads due to earthquakes, collisions and ship groundings, shallow cracks are also the ones most likely to reach full plasticity before crack extension. With this background, Lee and Parks (1993) developed a comprehensive set of accurate yield surfaces for plane strain SEC specimens. Consider a small geometry change continuum finite element model of the plane strain SEC specimen composed of an isotropic elastic–perfectly plastic material. Imposing sufficiently large magnitudes of δ and θ in fixed ratio on the top edge of their finite element models, they determined the limiting force and moment, and the vector (δ, θ) provided the corresponding yield surface normal vector at that limiting load point.

Figure 3 shows combined tension and bending yield surfaces in the generalized force space. The coordinates are normalized with shear flow strength τ_o and thickness t of the SEC specimen such that $\bar{Q}_1 = Q_1/2\tau_o t$; $\bar{Q}_2 = Q_2/\tau_o t^2$, and the corresponding normalized (plastic) displacements are $\bar{q}_1 = q_1/t$; $\bar{q}_2 = q_2/2$. With this normalization, the plastic dissipation rate per unit length can be expressed as $\dot{W}^p = Q_k \dot{q}_k = (2\tau_o t^2)\bar{Q}_k \dot{\bar{q}}_k$. Circled points are data numerically obtained from continuum finite element limit analyses (Lee and Parks, 1993). To satisfy convexity of the yield surface, solid lines were obtained by interpolating the sets of circled data points with a monotonic interpolant (Gregory and Debourgo, 1982). Subsequently, at fixed a/t, the values of yield surface normal and the radius for any particular load ratio $\bar{Q}_1/\bar{Q}_2$ are recovered by interpolation between tabulated a/t-values. We employ these improved yield surfaces in our elastic–plastic line-spring model described in the next section.

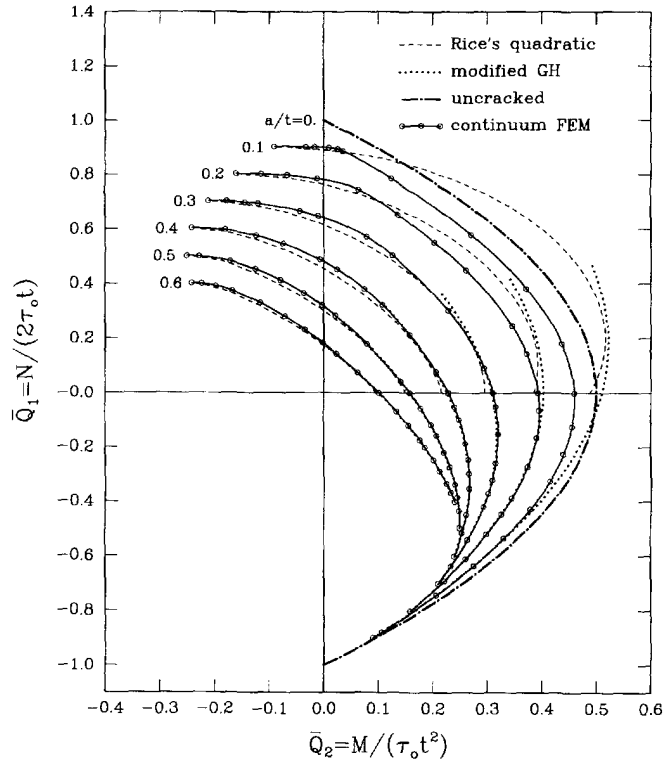

Fig. 3. Combined tension and bending yield surfaces in the generalized force space, the coordinates of which are normalized with the SEC specimen thickness t and shear flow strength τ_o. Solid lines (Lee and Parks, 1993) were interpolated from the set of circled data points. Also shown are the uncracked yield surface and Rice's quadratic forms (Rice, 1972a) and the modified Green and Hundy yield surfaces (White *et al.*, 1983).

Rice's quadratics (13) for predominant tension ($N > 0, \theta \geqslant 0$), modified GH solutions (14) for the range of axial force, $-2\tau_o l \leqslant N \leqslant 0.55 \cdot (2\tau_o l)$, and the uncracked yield surface (15) are also plotted in Fig. 3. Modified GH solutions show excellent agreement with numerically obtained yield surfaces down to relative crack depths of $a/t = 0.3$. For the very short crack depth $a/t = 0.1$, Rice's quadratics and the modified GH yield surface surpass the uncracked yield surface, which must include all true cracked yield surfaces. In application, accurate yield surfaces for a/t-values not in the yield surface data base are obtained by interpolation; one result is shown in Fig. 7.

2.3. *Elastic–plastic line-spring*

With the yield surface $\Phi(Q_i; a, t; \tau_o) = 0$ known in the generalized force space, together with an isotropic hardening assumption, the line-spring incremental constitutive relation for the fully plastic region can be constructed as follows.

The total generalized displacement increments Δq_i are additively decomposed into elastic and plastic parts: $\Delta q_i = \Delta q_i^{(e)} + \Delta q_i^{(p)}$. The elastic generalized displacement increments $\Delta q_i^{(e)}$ are represented in terms of the elastic compliance and the generalized force increments ΔQ_j:

$$\Delta q_i^{(e)} = P_{ij}(a, t)\Delta Q_j. \tag{16}$$

When the generalized force state is on the yield surface and active plastic loading occurs, the plastic generalized displacement increments are taken as the product of a non-negative scalar Λ and the outward yield surface normal

$$\Delta q_i^{(p)} = \Lambda \Phi_{,i} = \Lambda \frac{\partial \Phi}{\partial Q_i}. \tag{17}$$

Rewriting ΔQ_i and invoking the consistency condition that the force state remains on the yield surface during plastic flow leads to the following pair of equations, which are sufficient to describe "non-hardening" fully plastic behavior of the line-spring:

$$\Delta Q_i = S_{ij}(a, t)(\Delta q_j - \Lambda \Phi_{,j}) \tag{18}$$

$$\Phi = 0 \tag{19}$$

where $S_{ij}(a, t) \equiv P_{ij}^{-1}(a, t)$ represents the elastic stiffness matrix.

In case of hardening, we simply take the true stress/logarithmic plastic strain curve in uniaxial tension as the relation between the line-spring ligament-average flow strength, σ_o, and the ligament-average plastic strain, $\varepsilon_o^{(p)}$, so that in an incremental form

$$\Delta \sigma_o = \int_{\sigma_o}^{\sigma_o + \Delta \sigma_o} d\sigma_o = \int_{\varepsilon_o^{(p)}}^{\varepsilon_o^{(p)} + \Delta \varepsilon_o^{(p)}} h_s \, d\varepsilon_o^{(p)}. \tag{20}$$

The plastic material modulus h_s is the slope of the true stress/logarithmic plastic strain curve of the material in uniaxial tension.

Interpretation of the plastic work increment in two different ways associates $\Delta \varepsilon_o^{(p)}$ with $\Delta q_i^{(p)}$. At the macroscopic level, the plastic work increment per unit thickness of the SEC specimen $\Delta W^{(p)}$ is given by

$$\Delta W^{(p)} = Q_i \Delta q_i^{(p)}. \tag{21}$$

Another expression for this plastic work increment is given by the integral of the continuum plastic work increment over the area A of the SEC specimen where plastic dissipation is occurring

$$\Delta W^{(p)} = \int_A \sigma_{ij} \Delta \varepsilon_{ij}^{(p)} \, dA = \int_A \bar{\sigma} \Delta \bar{\varepsilon}^{(p)} \, dA. \tag{22}$$

Here the quantities $\bar{\sigma}$ and $\Delta\bar{\varepsilon}^{(p)}$ are local values of tensile equivalent stress and equivalent plastic strain increment in the dissipation area A. Parks (1981) inferred that the active plastic deformation area A of the deep crack would be proportional to the square of remaining ligament $l = (t-a)$. Although the slip-line field of the shallow crack can extend to the front surface, the plastic deformation area A is still proportional to the square of a "characteristic length"; thus we again choose the ligament l as the characteristic length, even for shallow cracks. Then, the last integral (22) can be evaluated approximately, in terms of σ_o and $\Delta\varepsilon_o^{(p)}$, as

$$\Delta W^{(p)} = f \cdot \sigma_o \cdot \Delta \varepsilon_o^{(p)} \cdot l^2 \tag{23}$$

where the dimensionless scalar f, which we call the *strain hardening factor*, is expected to be of order unity. On the assumption of isotropic hardening, equivalency of macroscopic and continuum plastic work increments provides

$$f \cdot \sigma_o \cdot \Delta \varepsilon_o^{(p)} \cdot l^2 = Q_i \Delta q_i^{(p)}. \tag{24}$$

Equations (18)–(20) and (24) represent a complete set of implicit incremental constitutive relations for fully plastic hardening behavior of the line-spring model [see also Parks and White (1982) for an explicit formulation in a rate form].

The value of f is calibrated by comparing the single line-spring behavior to the continuum finite element solution of a plane strain initial boundary value problem having the same dimensions, material properties and loading histories. For all continuum and line-spring finite element input data, we used a multi-linear stress–strain curve, smoothly approximating the experimental data of ASTM A710 Grade A steel. A parametric study of various crack depths under diverse loading conditions showed that the simple choice $f = 0.9$ enables the line-spring model to follow the continuum finite element solutions satisfactorily. Improving the line-spring compliances by use of effective crack length, tabulated yield surfaces, and a re-calibrated strain hardening factor finds its pay-off in a better evaluation of the crack-tip deformation parameters such as J, CTOD and crack-tip triaxiality as inferred or measured by the stress parameters T or Q.

The crack-tip deformation intensity parameter J is taken as the sum of an elastic and a plastic part; $J = J^{(e)} + J^{(p)}$. The effective value of elastic $J^{(e)}$ is estimated from (8). In the rigid–perfectly plastic case, the increment of $J^{(p)}$ is the product of the generalized displacement increments and the derivatives of the generalized limit loads with respect to the ligament length (Bucci *et al.*, 1972):

$$\Delta J^{(p)} = -\frac{\partial Q_i^{Lim}}{\partial a} \Delta q_i^{(p)} = \Lambda \Phi_{,i} \frac{\partial Q_i^{Lim}}{\partial l} \tag{25}$$

where the derivatives with respect to l of the generalized loads Q_i^{Lim} satisfying $\Phi = 0$ are taken at fixed $q_i^{(p)}$. Formally, (25) is restricted to rigid–perfectly plastic applications. In practice, however, the non-negative scalar Λ in our formulation already accounts (in a certain sense) for effects of strain hardening, so we continue to use (25) in hardening applications. The resulting form of J is quite approximate, but the magnitude of $J^{(p)}$ rapidly comes to dominate that of any conceivable definition of $J^{(e)}$, once gross plasticity prevails (Parks, 1981).

When test specimens or structures are under elastic–plastic situations, the displacement at any point in the body can be formally decomposed into its "linear elastic" and "plastic" parts. In this spirit, CTOD may be taken as the sum of two terms, an elastic and a plastic part; $\delta_t = \delta_t^{(e)} + \delta_t^{(p)}$. This additive form is also adopted in the ASTM E 1290 standard. The

"elastic" CTOD of a hardening material in plane strain small scale yielding condition is given by

$$\delta_t^{(e)} = d_n \frac{K_I^2}{H\sigma_y} = d_n \frac{J^{(e)}}{\sigma_y}. \tag{26}$$

In ASTM E 1290, the value of d_n is suggested as $d_n = 0.5$, which is close to small geometry change flow theory FEM results ($d_n \simeq 0.48$) by Tracey (1976) and Shih (1981), and large geometry change flow theory FEM results ($d_n \simeq 0.59$) by McMeeking (1977) and Wang (1991) for low to moderately hardening material. The plastic part of CTOD is related to the plastic parts of the load point displacement and rotation in incremental form (Parks, 1981) as

$$\Delta\delta_t^{(p)} = C_1(\alpha, a/t)\,\Delta\delta^{(p)} + C_2(\alpha, a/t)\cdot t\cdot\Delta\theta^{(p)} \tag{27}$$

where $\alpha \equiv \arctan(\bar{Q}_1/\bar{Q}_2)$ is the polar angle in Fig. 3, and a/t is relative crack depth. For a deeply cracked SEC specimen with slip-line fields confined to the ligament, the dimensionless functions C_i are given as $C_1 = 1$, $C_2 = 1/2 - a/t$ through a kinematical relation applicable to both an upper bound field (Rice, 1972a) and the modified GH slip-line field (White *et al.*, 1983). In deep crack configurations, the upper bound field is accurate for predominant tensile loading, and the modified GH slip-line field is effective for predominant bending loading conditions (see Fig. 3); thus the above values for C_i hold irrespective of loading condition. However, the values of C_i for shallow cracks are more complicated, as discussed by Lee and Parks (1993) [see also Figs 9 and 10 and the discussion below].

3. RESULTS

After being calibrated against continuum FEM analyses of plane strain SEC specimens, the modified line-spring model is applied to surface cracked plates. For unconditional stability in our numerical time integration procedure, we employed the Euler backward formulation so that the line-spring constitutive equations are satisfied at the end of a time increment.

3.1. *Plane strain SEC specimens*

Contained yielding region ($\Phi < 0$). Assuming Δq_i are given, the nonlinear implicit equations (4), (6), (7) and (12) are solved for Q_j with Newton–Raphson iterations for rapid convergence, and the integrals of eqn (12) are evaluated with ten-point Gaussian integration. Global equilibrium equations of the whole structure composed of shell and line-spring finite elements are also solved with Newton-type iterative methods (ABAQUS, 1988a); thus, we find the "elastic" Jacobian matrix $T_{ij}^{(e)} \equiv \partial Q_i/\partial q_j$ and send it to the main ABAQUS program. The detailed derivation of $T_{ij}^{(e)}$ is given in the Appendix.

Figure 4 shows the normalized axial force vs cracked displacement of the plane strain SEC specimen of relative crack depth $a/t = 0.5$ under remote pure tension ($N > 0$, $M = 0$; M is the moment about mid-specimen). Eight-node plane strain elements with reduced integration [element type CPE8R from the ABAQUS library (1988b)] were used for the continuum finite element model of the SEC specimen. In the continuum finite element solution, the uncracked displacement was subtracted from the total extension δ^{tot} to obtain the cracked displacement as a function of imposed load; $\delta^c = \delta^{tot} - 2L_s\cdot\hat{\varepsilon}(N/t)$, where $2L_s$ is the length of the SEC specimen and $\hat{\varepsilon}(N/t)$ represents the axial strain of the uncracked plane strain specimen subject to uniform axial stress (N/t). The PW line-spring model formulated with the actual crack length ($\beta = 0$), shows excellent behavior in the linear elastic region, but gradually deviates from the continuum solution as the imposed load increases. Among several modified line-spring solutions with β-values ranging from 0 to 0.26 in an increment of 0.065, the solution with $\beta = 0.13$ shows a good agreement with the

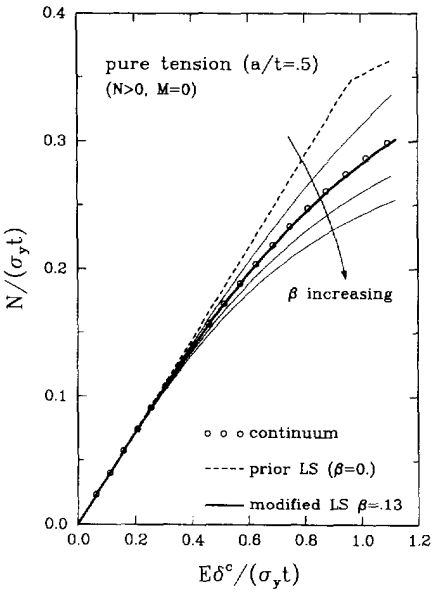

Fig. 4. Normalized axial force N vs cracked displacement δ^c of a plane strain SEC specimen of relative crack depth $a/t = 0.5$ under pure tension ($N > 0, M = 0$). The modified line-spring solution with $\beta = 0.13$ matches the continuum solution.

continuum solution. For the standard effective crack length form (6), Sham (1983) determined the asymptotic plastic zone size correction factor for a non-hardening material. When modified to account for material hardening with hardening exponent $n = 10$, which is employed in Fig. 4, Sham's work provides the value $\beta = 0.136$ (Hauf *et al.*, 1994). Since the limit load should be evaluated with actual crack length a, the effective crack length is used only up to the onset of fully plastic yielding, defined by $\Phi(Q_i; a, t; \tau_y) = 0$. Figure 5 shows the normalized axial force vs cracked displacement of the plane strain SEC specimen having relative crack depths $a/t = 0.5$, 0.35 and 0.2 under pure tension. Each curve is plotted up to near the onset of fully plastic flow. Solutions (Hauf *et al.*, 1994) based on the standard effective crack length formulation (6) are shown for comparison. For $a/t = 0.2$, a

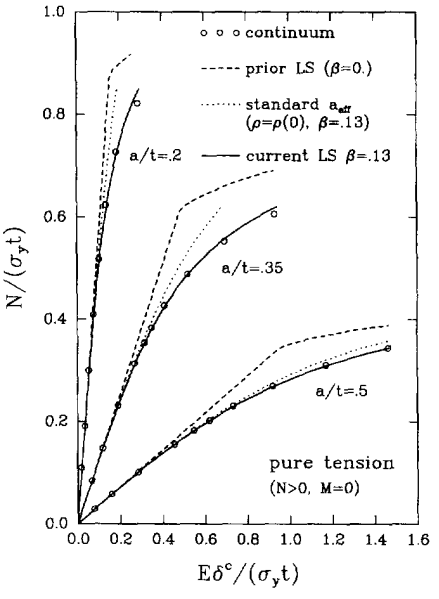

Fig. 5. Normalized axial force N vs cracked displacement δ^c of a plane strain SEC specimen under pure tension for relative crack depths $a/t = 0.5$, 0.35 and 0.2. Each curve is plotted up to near the onset of fully plastic yielding.

solution from the standard effective crack length formulation with $\rho = \rho(0) = 0.15$, and $\beta = 0.13$ fails to match the continuum solution at higher load levels.

Figure 6(a) shows the normalized J-integral vs cracked displacement for pure tension. The continuum J-value was obtained from the virtual crack extension/domain integral method (Li *et al.*, 1985; Parks, 1977) as implemented in the ABAQUS code (1988a). The variation in J over different domains in the continuum model was within 3%, an indication of the overall accuracy of the calculation. The J-value of the modified line-spring in the transition region is obtained by $J = K_I^2(a_{\text{eff}})/H$, and the improvement obtained by accounting for the effects of T-stress on a_{eff} as per (4)–(9) is evident, especially in the shallow cracked geometries where T-stress is inherently negative. In Fig. 6(b) the normalized J-integral is plotted against the axial force for pure tension, and again the modified line-spring solution with $\beta = 0.13$ matches the continuum solution exceptionally. Figures 6(a) and (b) illustrate that excessive elastic stiffness of the PW line-spring formulation generally causes overestimates of J for a given imposed displacement, and underestimates of J for a given load parameter in the intermediate scale yielding region.

Fully plastic region ($\Phi = 0$). Within the context of the Euler backward formulation, the elastic–plastic line-spring constitutive relations are given by the set of nonlinear implicit equations (18)–(20) and (24). At the beginning of a time increment, estimates of Δq_i are presumed known. For given Δq_i, we assume $\Delta q_i^{(p)}$, and find the corresponding ΔQ_i from (18). Then, $\Delta\varepsilon_0^{(p)}$ and $\sigma_0(\varepsilon_0^{(p)} + \Delta\varepsilon_0^{(p)})$ are determined from the work equivalency equation (24) by Newton–Raphson iterations. Finally, $\Delta q_i^{(p)}$ and $\Delta\varepsilon_0^{(p)}$ are corrected [by $\mathrm{d}(\Delta q_i^{(p)})$ and $\mathrm{d}(\Delta\varepsilon_0^{(p)})$, respectively] to satisfy the normality (17) and consistency (19) conditions. Corrected values of the plastic displacement increments $[= \Delta q_i^{(p)} + \mathrm{d}(\Delta q_i^{(p)})]$ are substituted for assumed values of $\Delta q_i^{(p)}$ above, and the remaining steps are repeated until the corrections $\mathrm{d}(\Delta q_i^{(p)})$ are within specified tolerances, or equivalently, until the four implicit constitutive equations (18)–(20) and (24) are satisfied simultaneously. Subsequently, we find the elastic–plastic Jacobian matrix $T_{ij}^{(ep)} \equiv \partial Q_i/\partial q_j$, which is used for revising the estimates of nodal displacements Δq_i in main ABAQUS [see the Appendix for details of definition and derivation of $T_{ij}^{(ep)}$].

The normalized axial force vs cracked displacement curves of the plane strain SEC specimen for various relative crack depths ($a/t = 0.5$, 0.35 and 0.2) under remote pure

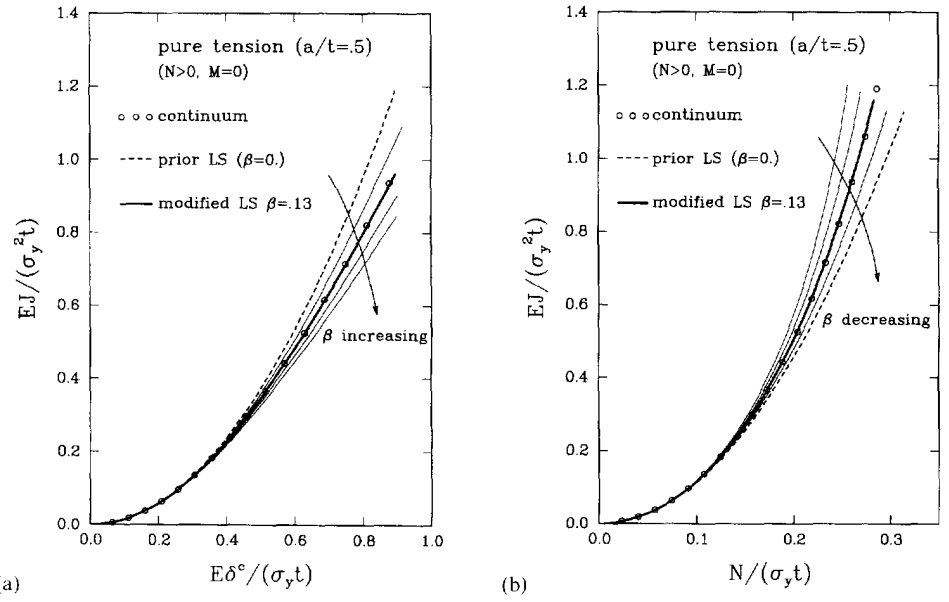

Fig. 6. Normalized J vs cracked displacement (a), and normalized J vs axial force (b) of a plane strain SEC specimen of relative crack depth $a/t = 0.5$ under pure tension. The effective J-value of the modified line-spring in this transition region is obtained from K_I (a_{eff}) using eqn (8) directly.

tension are shown in Fig. 7. Three curves, the previous (PW) line-spring solution, the modified line-spring solution and the continuum solution, are plotted for each crack depth. The PW solutions, which are based on Rice's approximate yield surface and strain hardening factor $f = 0.4$, tend to deviate from the continuum solutions and reach limiting loads somewhat early. Note that Rice's quadratics underestimate limiting load values near pure tension loading, as shown in Fig. 3, and this is reflected in Fig. 7. For the modified line-spring model equipped with effective crack length and with more accurate tabulated yield surfaces, parametric study of the strain hardening factor demonstrated that the constant value of $f = 0.9$ generally produces acceptable agreement between continuum and line-spring load–displacement histories, such as mid-ligament tension ($N > 0$, $\theta = 0$), pure tension ($N > 0$, $M = 0$), and pure bending ($N = 0$, $M > 0$). The nonlinearities in the transition region are again captured by the effective crack length. The yield surface of, for example $a/t = 0.35$, was linearly interpolated between tabulated yield loci of $a/t = 0.4$ and $a/t = 0.3$, and the validity of this simple linear interpolation between crack depths is corroborated by the accuracy of the load–displacement curve for $a/t = 0.35$.

Figure 8 shows the normalized J-integral vs the generalized force for the relative crack depths $a/t = 0.5$ and 0.2 under mid-ligament tension loading. For a deep crack of $a/t = 0.5$, three solutions fall on almost the same locus, while for the shallow crack of $a/t = 0.2$, only the modified line-spring solution traces the path of the continuum solution closely, and the improvement is noteworthy. Figures 7 and 8 indicate that the effective crack length correction parameter $\beta = 0.13$ and the re-calibrated strain hardening factor $f = 0.9$ might be accepted for a range of relative crack depths and load histories, at least within the scope of the adopted formulation for moderate strain hardening, $n = 10$.

Plastic CTOD. Investigating the upper bound flow field, modified GH slip-line field, and some general features of the yield surfaces, Lee and Parks (1993) took C_1 as equal to unity, then recast eqn (27) in the form

$$\Delta\delta_t^{(p)} = \Delta\delta^{(p)}\left[1 + L_2 \cdot \left(\frac{1}{2} - \frac{a}{t}\right) \cdot \left(\frac{t\Delta\theta^{(p)}}{\Delta\delta^{(p)}}\right)\right]. \tag{28}$$

Here $L_2 = \hat{L}_2(a/t, \psi) = C_2/(1/2 - a/t)$, $\psi(\alpha) = \arctan(2\Delta\delta^{(p)}/t\Delta\theta^{(p)})$ is the angle between the

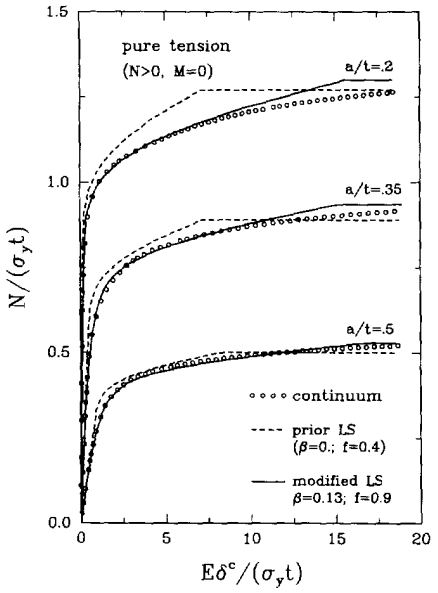

Fig. 7. Normalized axial force N vs cracked displacement δ^c of plane strain SEC specimens of relative crack depths $a/t = 0.5$, 0.35 and 0.2 under pure tension ($N > 0, M = 0$).

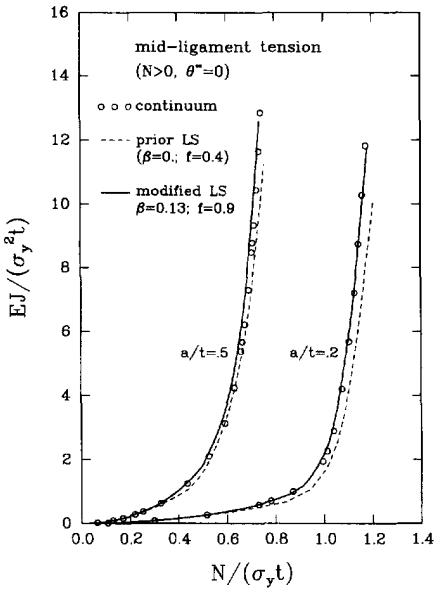

Fig. 8. Normalized J vs axial force N for mid-ligament tension ($N > 0, \theta = 0$) of plane strain SEC specimens of relative crack depths $a/t = 0.5$ and 0.2. The ratio of specimen length to thickness is $2L_s/t = 6$. The improvement in the solution of the shallow crack ($a/t = 0.2$) is due to accurate tabulated yield surfaces and the newly calibrated value of $f = 0.9$.

yield surface normal and the horizontal axis in the normalized force space of Fig. 3, and $\alpha \equiv \arctan(\bar{Q}_1/\bar{Q}_2)$ again.

Figure 9 shows the function L_2 plotted against the ratio of plastic displacement increments, from mid-ligament tension to its mirror image of mid-ligament compression (Lee and Parks, 1993). For sufficiently deep cracks, $a/t \geqslant 0.4$, $L_2 = 1$ throughout the whole range, while for shallow cracks ($a/t \leqslant 0.3$), L_2 shows a 'V'-shape variation, indicating a strong interaction between crack-tip and front surface. The plastic CTOD increments in the PW line-spring model are calculated based on $L_2 = 1$ for all crack depths. As is clear from Fig. 9, however, using constant $L_2 = 1$ is not advisable when $L_2 \ll 1$. Thus, $L_2 = \hat{L}_2(a/t, \psi)$ was incorporated into our line-spring model for a better estimation of the plastic CTOD.

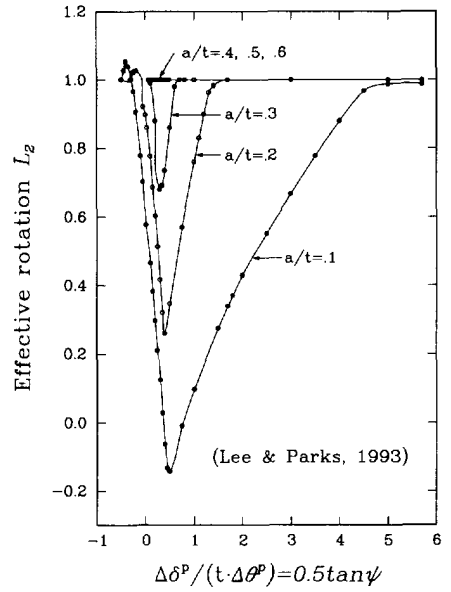

Fig. 9. Crack-tip opening displacement function L_2 [see (28)] vs ratio of load point plastic displacement increments for various relative crack depths [from Lee and Parks (1993)]. Function $L_2(a/t, \psi)$ represents the degree of negative relative rotation of the crack flank.

The normalized CTOD vs the generalized force for the relative crack depths $a/t = 0.5$ and 0.2 under pure tension are plotted in Fig. 10. CTOD in the continuum model is defined as the opening distance between the intercept of the two 45° lines, drawn back from the tip in the deformed configuration (Tracey, 1976), and this operational definition was applied to continuum FEM solutions to obtain corresponding values of CTOD. Both the PW and the modified line-spring solutions show fairly good agreement with the continuum solutions for the deep crack of $a/t = 0.5$. For the shallow crack of $a/t = 0.2$, the PW model considerably underestimates the CTOD value in the general yielding region, and attains an excessive limit load (vertical line). On the other hand, the modified line-spring model accurately tracks the continuum solutions up to the limit load, and consequently shows substantial improvement.

3.2. *Surface cracked plates*

J-distributions along crack fronts. The surface cracked plate which was analysed is schematically shown in Fig. 1. The plate has a length $2h$, a width $2b$ and a thickness t, with $h/t = 16$ and $b/t = 8$. The semi-elliptical crack in the center of the plate has a surface length $2c$ and a maximum through-thickness penetration a. The parametric angle ϕ locates position along the semi-elliptical crack front. Eight-node shell elements with reduced integration [element type S8R from the ABAQUS library (1988b)] were used to model one quarter of the plate in Fig. 1. To secure an adequate elastic–plastic compliance in response to the remote bending moment, eleven Simpson's rule integration points across the thickness of the shell were used. Ten three-node second order line-spring elements assuming a symmetry plane cross the spring were placed to represent the cracked plane.

Figures 11(a) and (b) show the normalized J-distribution along the crack front of the surface cracked plate having $a/t = 0.6$ and $a/c = 0.24$ under a remote tension and a remote bending moment, respectively. Open circles represent 3-D continuum finite element solutions (Wang, 1991) performed with the same stress–strain model of ASTM A710 Grade A steel, and solid lines are the current line-spring solutions. For the remote tension case ($\delta^{\infty} > 0$, $\theta^{\infty} = 0$), the load level was defined as the ratio of remote displacement to the displacement at general yielding of the uncracked cross section, i.e. $\mathscr{E}^{\infty} \equiv E \cdot \delta^{\infty}/(2h\sigma_y)$. For remote bending ($\theta^{\infty} > 0, N^{\infty} = 0$), the load level was measured by the ratio of remote moment per unit width to the moment per unit width at general yielding of the uncracked cross section, or $\Sigma^{\infty} \equiv M^{\infty}/(\sigma_y t^2/4)$.

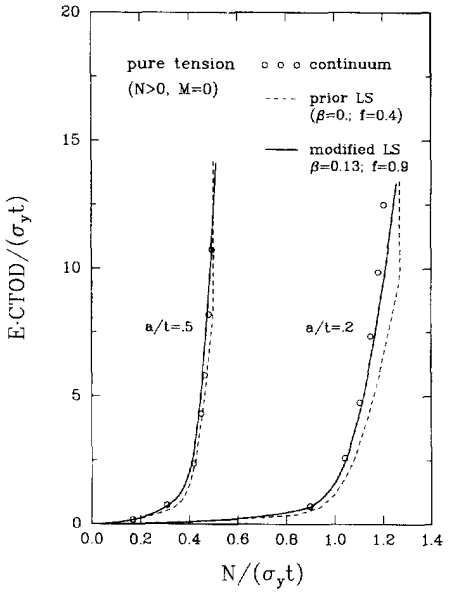

Fig. 10. Normalized CTOD vs axial force N for pure tension ($N > 0, M = 0$) of plane strain SEC specimens of relative crack depths $a/t = 0.5$ and 0.2. The incorporated function L_2 and tabulated yield surfaces improve the shallow crack results.

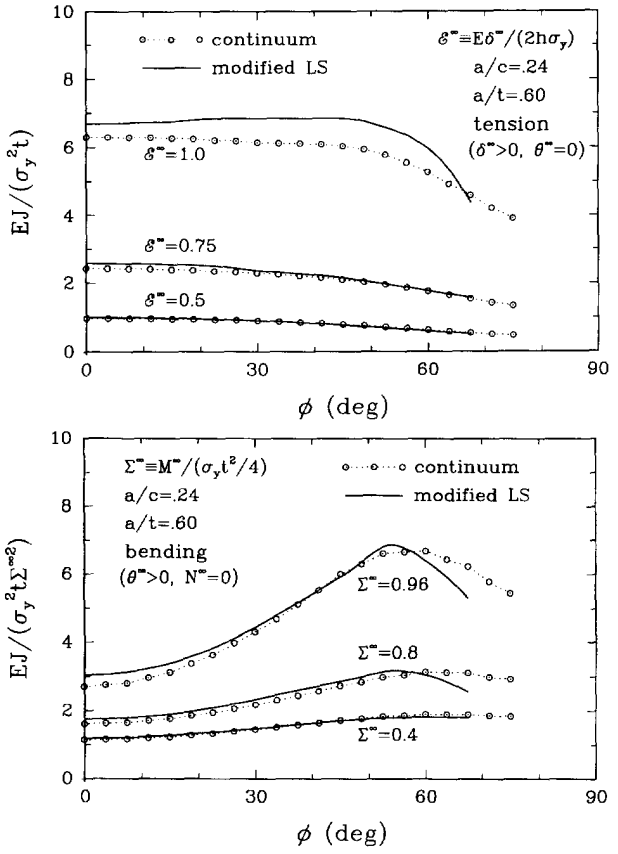

Fig. 11. Normalized J along the crack front of surface cracked plate under remote tension (a), and remote bending (b) at various remote load levels. With respect to Fig. 1 schematic, "tension" denotes ($N^{\infty} > 0, \theta^{\infty} = 0$), while "bending" is ($M^{\infty} > 0, N^{\infty} = 0$). For both solutions, $h/t = 16$ and $b/t = 8$.

Up to intermediate load levels ($\mathscr{E}^{\infty} = 0.75$ and $\Sigma^{\infty} = 0.8$), the modified line-spring solutions match the 3-D continuum solutions along most of the surface crack front. Even at fully plastic load levels ($\mathscr{E}^{\infty} = 1.0$ and $\Sigma^{\infty} = 0.96$), the agreement between the two solutions is still quite acceptable for both loading conditions. We note that at $\mathscr{E}^{\infty} = 1.0$, center-line CTOD $\approx 0.02l$, which is near the limits of a crack mechanics approach. As the level of applied tensile load increases, the plastic zone penetrates the ligament to reach the back surface of the plate, and, simultaneously, gross shear banding can evolve in the plate, passing through the intersection of the crack front with the front surface (Dodds and Read, 1990). While the former pattern of deformation is accommodated by line-spring elements, the latter one must be accommodated by shell elements of the plate model. We did not take special measures in our definition of the shell FEM mesh to include this in-plane shear effect into the plate model. Near the intersection of the in-plane shear band with the ends of the model surface crack, lack of sufficient shell mesh compliance caused a sharp drop of line-spring estimates of J-integral values, under large scale yielding, as compared with the continuum solutions.

Crack opening stress. When the surrounding elastic field is modeled by the first two terms of the Williams expansion, the stress field deep inside the plastic zone is known as modified boundary layer (MBL) solution (Larsson and Carlsson, 1973). Studies on the MBL solution have shown that crack opening stress can be quantitatively correlated with two parameters, J and the normalized T-stress (Betegón and Hancock, 1991; Wang, 1993).

Parks (1991) proposed that the crack opening stresses σ_{22} ($= \sigma_{\theta\theta}$ at $\theta = 0$) in any plane perpendicular to a 3-D crack front can be characterized by the modified boundary layer (MBL) solution,

$$\frac{\sigma_{22}^{3\text{-D}}(r/(J(\phi)/\sigma_y);\tau(\phi))}{\sigma_y} \doteq \frac{\sigma_{22}^{SSY}(r/(J(\phi)/\sigma_y))}{\sigma_y} + A_n\tau(\phi) + B_n\tau^2(\phi) + C_n\tau^3(\phi). \quad (29)$$

Here, in the local coordinate system (x_1, x_2, x_3), the x_1–x_2 plane is perpendicular to the crack front, whereas the x_3-axis is tangential to the crack front. The local polar coordinates (r, θ) are in the plane of $(x_1$–$x_2)$, and $\theta = 0$ when $x_2 = 0$ and $x_1 > 0$. The stress on the left hand side of (29) is the crack opening stress in a surface cracked plate at crack front location ϕ and normalized distance $r/(J/\sigma_y)$ ahead of the crack front. The right hand side of (29) is the MBL solution at the same normalized distance (Betegón and Hancock, 1991; Wang, 1993). The small scale yielding (SSY) solution can be interpreted as a particular value of the MBL solution at $\tau = 0$. The constants A_n, B_n and C_n depend upon the strain hardening exponent n of the material, and $\tau(\phi) \equiv T(\phi)/\sigma_y$. The choice of normalized distance $r/(J/\sigma_y)$ has little effect on the fitted constants as long as it is outside the blunting zone (Betegón and Hancock, 1991), but suitably small compared to local uncracked ligament.

At the distance $r = 2J/\sigma_y$, Wang (1993) fitted the MBL solution with $(A_n, B_n, C_n) = (0.6168, -0.5646, 0.1231)$ for a material having $n = 10$ and $\nu = 0.3$. In Fig. 12, the center plane ($\phi = 0^\circ$) crack opening stresses at $r/(J/\sigma_y) = 2$ are plotted against $\Sigma^\infty \equiv N^\infty/\sigma_y t$, for the deeply cracked plate under remote tension. Here $\Sigma^\infty \equiv N^\infty/\sigma_y t$ is the remotely applied force per unit width normalized by the membrane force at general yielding of the uncracked cross section. HRR and SSY solutions at $r/(J/\sigma_y) = 2$ are invariant; that is, $\sigma^{HRR} = 3.59\sigma_y$ and $\sigma^{SSY} = 3.34\sigma_y$ for the given $n = 10$ (Wang, 1993). Both the 3-D FEM solution (Wang, 1993) and the LS/MBL solution, which is directly inferred from the load history of each line-spring, show a steady decrease in magnitude as the applied load increases. In the LS/MBL solution, the T-stress variation along the crack front $T(\phi)$ is obtained by inserting our modified elastic–plastic line-spring solutions Q_i into eqn (9). Up to load level $\Sigma^\infty = 0.98$, the LS/MBL solution is in distinguished agreement with 3-D FEM solution, at least for the given crack configuration and loading type.

Figure 13 shows the distributions of the crack opening stress at $r/(J/\sigma_y) = 2$, normalized by the predicted values $\sigma^{LS/MBL}$ along the crack front for remote tensile loads ranging from SSY to limit load. Data at $\phi > 60^\circ$ are not included because both the 3-D FEM solution (Wang, 1993) and the line-spring solution are not adequately refined in this region, where the fields vary rapidly as the crack depth changes in a precipitous manner. However, the physical extent of crack front included in $60^\circ < \phi < 90^\circ$ is very small because of the low aspect ratio ($a/c = 0.24$). For $\Sigma^\infty < 0.925$, the agreement between two solutions is better than 98% along most of the crack front. Even at $\Sigma^\infty = 0.980$, the LS/MBL prediction is still within 5% of the 3-D finite element solution. The results in Figs 12 and 13 demonstrate

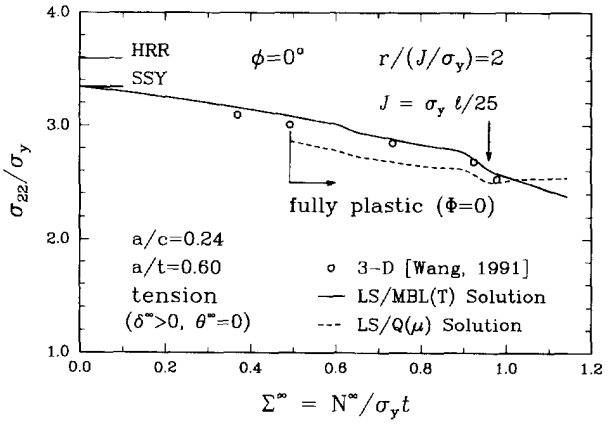

Fig. 12. Center plane ($\phi = 0^\circ$) crack opening stress at $r = 2J/\sigma_y$ vs remote load level $\Sigma^\infty \equiv N^\infty/\sigma_y t$ for surface cracked plate under remote tension. The solid line denotes a line-spring prediction based on calculated values of T-stress and the MBL correlation of σ_{22} with T/σ_y. The dashed line is an approximate fully plastic estimate based on the dependence of σ_{22} in deeply cracked non-hardening SEC specimen to the (evolving) tension to bending ratio within the line-spring [see (30)–(33)].

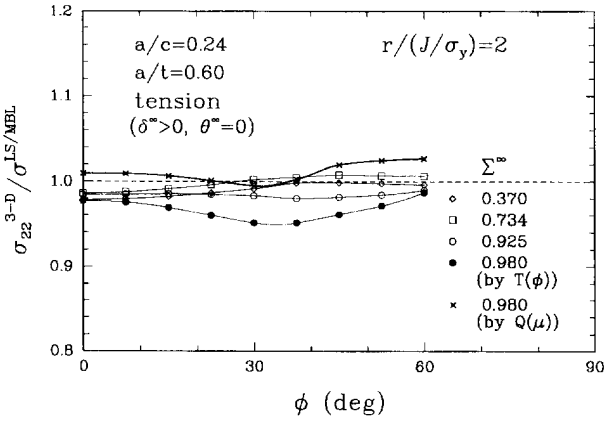

Fig. 13. Crack opening stress normalized by LS/MBL solution, plotted along the crack front, at various load levels for a surface cracked plate under remote tension. Cross symbols '×' represent the crack opening stress normalized by the fully plastic line-spring estimate using $Q(\mu)$ obtained from eqn (33).

that the simplified line-spring model successfully estimates elastic–plastic crack front fields with a variety of constraints, in agreement with similar results by Wang (1993) based on the PW line-spring.

Fully plastic estimate of stress triaxiality. The results in Figs 12 and 13 show that "elastically calculated" estimates of the T-stress, in conjunction with MBL solutions, provide very accurate estimates of stress triaxiality in surface cracked plates, even up to fully plastic conditions. Under fully plastic ligament conditions this success comes despite the fact that there simply is no elastic zone surrounding the crack front. This lack of formal basis for continued use of T and MBL correlations in estimating local crack-tip stress triaxiality has been criticized by O'Dowd and Shih (1991, 1992), who advocate a local description of the crack-tip fields based on a reference solution, σ_{ij}^{REF}, and the so-called Q-stress parameter:

$$\sigma_{ij} \doteq \sigma_{ij}^{\text{REF}} + Q\sigma_y\delta_{ij} \quad \text{for} \quad r > J/\sigma_y, \quad |\theta| < \pi/2. \tag{30}$$

Here, either the HRR fields (σ_{ij}^{HRR}) or the SSY fields (σ_{ij}^{SSY}) can be chosen as σ_{ij}^{REF}, and Q is operationally defined as the difference between the crack-tip opening stress of the full-field solution and $\sigma_{22}^{\text{REF}}(r = 2J/\sigma_y, \theta = 0)$. The parameter Q can always be extracted from sufficiently detailed finite element solutions, but this can become cumbersome for 3-D solutions. Under contained yielding conditions, Q is isomorphic to T/σ_y, so that accurate values of Q can be rigorously generated from T, the latter of which is easily calculated (Nakamura and Parks, 1992; Parks, 1992; Wang and Parks, 1992). In fully plastic loading, no comparably simple, generally applicable methods for calculating Q exist. However, accurate estimates of fully plastic Q-values for deeply cracked plane strain SEC specimens under combined tension and bending can be obtained in a simple manner.

Let the parameter μ measure the bending to tension ratio applied to an edge cracked specimen as

$$\mu \equiv \frac{M + Na/2}{Nl}, \tag{31}$$

where $(M + Na/2)$ is the bending moment about the mid-ligament of the SEC specimen. The value of μ ranges from zero for mid-ligament tension to infinity for pure bending. Kim *et al.* (1994b) applied a least upper bound field consisting of slip on a circular arc, and showed that the angle θ_s at which the arc intersects the crack-tip depends on μ. Assuming the normal traction on the optimal arc satisfies the Hencky equilibrium equation, they

further showed that σ_s, the normal stress across the optimal arc at the crack-tip, could be expressed in terms of μ. Finally, Lee and Parks (1993) extended the partial Prandtl fields of Du and Hancock (1991), using the hydrostatic stress σ_s at angle θ_s to provide the non-hardening crack opening stress σ_{22} on $\theta_s = 0$ as

$$\sigma_{22} = \sigma_s + 2\tau_y\left(\theta_s - \frac{\pi}{4}\right) + \tau_y. \tag{32}$$

This simple estimate was shown to agree very well with finite element limit load solutions over a range of μ; Fig. 14 shows the agreement. The peak value of σ_{22}, occurring for $\mu \geqslant 0.6$, is $2.91\sigma_y$. Thus, with this value as non-hardening reference stress, we may write

$$Q(\mu) = \sigma_{22}(\mu)/\sigma_y - 2.91 \quad \text{for} \quad 0 \leqslant \mu \leqslant 0.6. \tag{33}$$

Strictly, (33) is predictive for Q in non-hardening, fully plastic deeply cracked SEC specimens. O'Dowd and Shih (1992) hypothesized that the fully plastic non-hardening $Q(\mu)$-values could be used in applications with low levels of hardening.

Figure 15 shows crack opening stress profiles for a material having a power law exponent $n \doteq 10$, in SEC specimens subject to increasing loads at fixed values of μ. Limit load was estimated based on the average flow stress, approximately $1.2\sigma_y$. Dashed lines represent load levels giving $25J/\sigma_y \geqslant l$, while dotted lines are for solutions within the fully plastic regime $\Phi < 0$. The solid lines are for solutions satisfying both {load > limit load} and $\{25J/\sigma_y < l\}$. These solutions are most appropriate for fracture mechanics assessments of fully plastic stress triaxiality, since conditions of gross blunting outside the realm of crack mechanics are excluded. Also shown are HRR crack opening stress for $n = 10$ and the shifted profiles based on (30), with HRR as reference and using the non-hardening fully plastic $Q(\mu)$ estimate of (33). The estimates are remarkably accurate for the low μ-values $0 \leqslant \mu \leqslant 0.3$ (tension dominant), but deteriorate somewhat as bending increases ($\mu = 0.4$, 0.5). On the other hand, at least part of the discrepancy at larger bending is due to the impingement of the crack tip zone into the fully plastic ligament-bending region, as evidenced by marked lack of "parallelism" of the HRR and continuum profiles. Indeed, the lack of "parallel shift" in crack opening profiles under high bending leads to a pronounced radial dependence of Q which is inconsistent with (30).

Finally, the $Q(\mu)$-based fully plastic estimation procedure for crack opening stress was applied to the surface cracked line-spring solutions in Figs 12 and 13. Figure 12 shows the center-line estimates at global loads for which the central spring satisfied $\Phi = 0$; they are

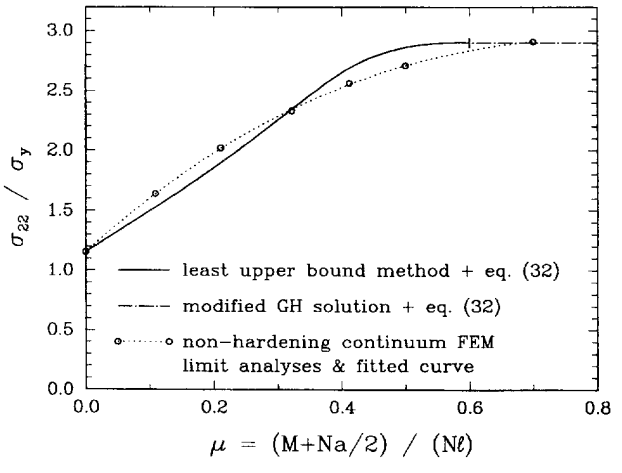

Fig. 14. Crack opening stress σ_{22} at the crack-tip of a non-hardening, plane strain deeply cracked SEC specimen as a function of remotely applied net section tension to bending ratio, μ. Least upper bound method solution from Kim *et al.* (1994b).

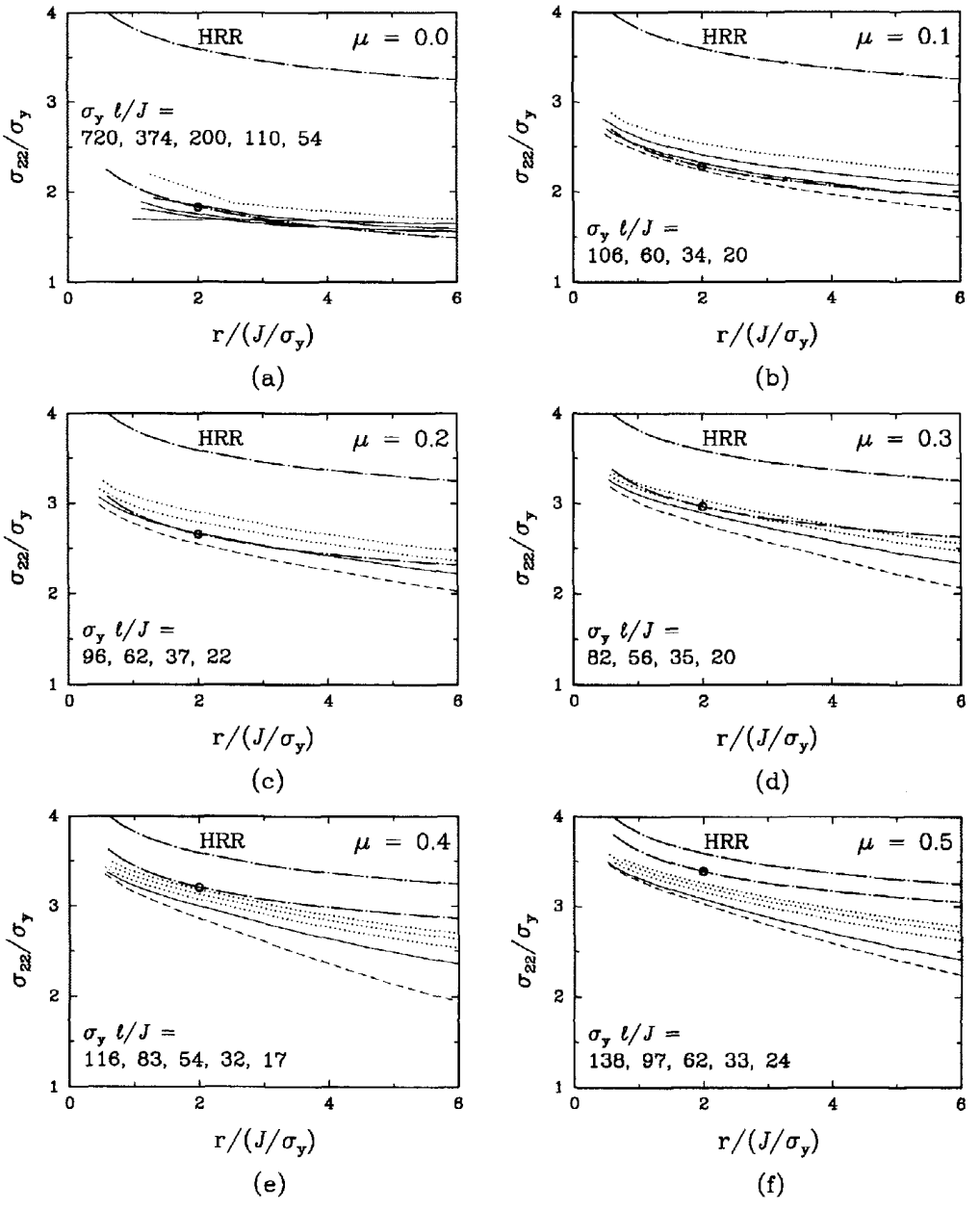

Fig. 15. Crack opening stress profiles in a plane strain deeply cracked SEC specimen having $a/t = 0.5$ for a material with $n = 10$. The applied bending to tension ratio is represented by the parameter μ. Dashed lines represent load levels giving $25J/\sigma_y \geq l$, while dotted lines are for solutions within the fully plastic regime $\Phi < 0$. The solid lines are for solutions satisfying both {load > limit load} and $\{25J/\sigma_y < l\}$. Also shown are HRR crack opening stress for $n = 10$ and the shifted profiles based on (30), with HRR as reference and using the non-hardening fully plastic $Q(\mu)$ estimate of (33), represented by the circle.

slightly below the line-spring estimates based on T, except at the highest loads. The predicted trend of the fully plastic results saturates at high load, in contrast to those based on T. While the former trend is expected, the continuum FEM solutions do not extend to higher loads; in any event, the local J exceeds $\sigma_y l/25$ for $\Sigma^\infty > 0.95$. The results in Fig. 13 shown with the '×' symbol give the predicted crack opening stress distribution along the surface crack at $\Sigma^\infty = 0.98$, where all elements satisfy $\Phi = 0$, based on the line-spring μ-values and

the fully plastic, strain hardening $Q(\mu)$ estimates presented. The overall accuracy of the predictions exceeds that of the line-spring predictions based on T.

4. DISCUSSION

The main requirements of an analytical or computational model in fracture mechanics are two fold: to describe the stress and deformation state at the crack front in terms of structural and crack geometry, applied loading, and material properties, and to provide an appropriate description of the macroscopic response of a structure or component containing a crack. In fulfilling these objectives, there are a range of models and analysis procedures, of varying complexity and sophistication, which are used in engineering practice. The choice of model in a given circumstance depends critically on the context in which the analysis is posed. Among the important contextual issues considered are the required level of accuracy in describing the cracked structures, and the costs associated with obtaining that level of accuracy. In this vein, the line-spring model has proven to be an effective compromise of accuracy and cost for analysis of part-through surface cracks in plate and shell structures. We have improved the accuracy of the model, with negligible additional cost, in four important ways.

First, the adoption of a novel effective crack length formulation provides substantially improved accuracy in estimates of structural compliances and of crack front deformation intensity (as measured by J and CTOD), for cases of contained plasticity. The new effective crack length formulation, which accounts for the strong influences of normalized T-stress on the size of crack-tip plastic zone (Larsson and Carlsson, 1973; Rice, 1974; Betegón and Hancock, 1991; O'Dowd and Shih, 1991; Wang, 1993), greatly enhances the accuracy of the model, especially for cases where T-stress is negative. This situation occurs for shallow cracks loaded in tension and bending, and for deeper surface cracks loaded in tension (Wang and Parks, 1992). Further results of the new effective crack length formulation, not limited to combined tension and bending of SEC geometries, can be found in Hauf *et al.* (1994).

In the regime of contained yielding, the T-stress is an effective correlator of the triaxiality of the stress deep within the crack-tip plastic zone. For plane strain SEC specimens subject to combined tension and bending, local crack opening stress profiles have been well predicted by T-based approaches for essentially all relative crack depths, and for load levels up to the point of impingement of fully plastic "global bending" fields into the crack-tip region (Betegón and Hancock, 1991; Sharma *et al.*, 1994; Wang and Parks, 1994). Indeed, the effectiveness of a T-stress correlation of local stress triaxiality was demonstrated for both deep and shallow surface cracked plates subject to both tension and bending by Wang (1993) in the continuum FEM sense, and within a line-spring model, by Wang and Parks (1992). Our results are fully consistent with those cited.

Secondly, in the fully plastic regime, accurate estimates of structural compliance require accurate estimates of limit load. The recent plane strain limit load solutions (Lee and Parks, 1993) of combined tension and bending geometries have greatly improved the fully plastic modeling of shallow cracks ($a/t \leqslant \sim 0.35$). Previous limit analyses based on the deep crack feature of deformation confined to the uncracked ligament (Rice, 1972a; Kim *et al.*, 1994a,b), while accurate for deep cracks, overestimate the load-carrying capacity of shallow cracks; this feature carries over to line-spring estimates as well. Moreover, since plastic deformation breaks back to the front surface in fully plastic shallow cracked SEC specimens, deep crack estimates of crack tip deformation intensity (CTOD) in terms of remotely imposed extension and rotation are gross overestimates (Lee and Parks, 1993). The current line-spring formulation correctly accounts for these features (Figs 8 and 10).

Third, ligament-average work hardening in the fully plastic regime is addressed in the manner proposed by Parks (1981), through the use of a dimensionless coefficient f, whose value can be argued to be of order unity on dimensional grounds. Parks and White (1982) calibrated the prior line-spring model based on the crude, trilinear model of stress–strain response and suggested $f \doteq 0.4$ as appropriate. Here, using the improved yield surfaces of Lee and Parks (1993) and a more realistic stress–strain model (near power law hardening,

with hardening exponent $n = 10$), we find that the simple choice $f = 0.9$ provides good overall results. In general, however, the parameter f should be considered as possibly depending on the details of the solutions, including level of strain hardening, relative crack depth, and magnitude and type of imposed loading. Further research into these issues may be merited.

Lastly, we addressed the issues of predicting crack-tip stress triaxiality in the fully plastic range for deep cracked plane strain SEC specimens under combined tension and bending, based directly on (approximate) fully plastic solutions. The crack opening stresses of non-hardening finite element limit analyses (Lee and Parks, 1993) correlate well with an approximate closed form expression derivable from a family of least upper bound solutions (Kim *et al.*, 1994b). For non-hardening line-spring applications, either of these approaches directly provides accurate estimates of the Q-stress in terms of the imposed bending to tension ratio for those crack front locations which are fully plastic. Following a suggestion of O'Dowd and Shih (1992), we extended the application of non-hardening estimates of crack tip stress triaxiality in SEC specimens to obtain the corresponding estimates for the cases of low strain hardening. The simple procedure adopted was to shift the reference value of peak non-hardening stress triaxiality (under dominant bending) to match the HRR reference value for hardening. Figure 15 shows the generally good predictions of the model in matching fully plastic crack opening stress profiles for various bending to tension ratios. When the procedure is applied to estimate crack opening stress in the surface cracked plates, the Q-based fully plastic estimates are close to both continuum solutions and to those based on the "elastically calculated" T-stress through the MBL correlation (Figs 12 and 13). There are indications that at the highest levels of plasticity, the accuracy of the fully plastic estimates of Q exceeds that of estimates based on T and MBL correlations.

5. SUMMARY

To capture the nonlinearity of the load–displacement curve in the intermediate yielding region, a new effective crack length formulation was introduced, and it provided smooth transition of the compliances and deformation parameters between linear elastic and fully plastic regions. The modified effective crack length solutions matched the continuum solution to higher fractions of limit load, and distinguished themselves from both LEFM and standard effective crack length solutions. Accurate tabulated yield surfaces were adopted, and together with the re-calibrated strain hardening factor $f = 0.9$, they enhanced the fully plastic line-spring behavior, especially in shallow crack configurations. The effect of front face plasticity on the plastic CTOD of shallow cracks was incorporated into the fully plastic line-spring model by using the calibrated function L_2. Applications to surface cracked plate problems showed that the line-spring model can be used to predict accurately the deformation (J, CTOD) and the wide range of crack-tip stress triaxiality along the surface crack front fields. For a low hardening material ($n = 10$) under a load state below the limit load, the line-spring element provides for direct inference of the crack-tip stress triaxiality from (9), the T-stress, together with the MBL correlations of stress triaxiality with T. For the fully plastic non-hardening deep crack case, the line-spring element can measure the crack-tip constraint from (33), $Q(\mu)$, and this fully plastic approach can be also used for an approximate evaluation of crack-tip constraint in a low hardening material under fully plastic loading.

Acknowledgments——This work was supported by the Office of Basic Energy Sciences, Department of Energy, under Grant No. DE-FG02-85ER13331. Computations were performed on an Alliant FX-8 computer obtained under DARPA Grant No. N00014-86-K-0768, and on Sun Sparc workstations obtained under ONR Grant No. 0014-89-J-3040. The ABAQUS finite element program was made available under academic license from Hibbitt, Karlsson and Sorensen Inc., Pawtucket, RI, and the assistance of Dr P. Burgers of HKS Inc. is gratefully acknowledged. Thanks are also due to Dr Y.-Y. Wang of Edison Welding Institute for providing us with the 3-D surface crack solutions.

REFERENCES

ABAQUS (1988a). Theory Manual, Version 4-8-1. Hibbitt, Karlsson and Sorensen, Inc., Providence, RI.
ABAQUS (1988b). User's Manual, Version 4-8-1. Hibbitt, Karlsson and Sorensen, Inc., Providence, RI.

Betegón, C. and Hancock, J. W. (1991). Two-parameter characterization of elastic–plastic crack tip fields. *J. Appl. Mech.* **58,** 104–110.

Bucci, R. J., Paris, P. C., Landes, J. D. and Rice, J. R. (1972). *J*-integral estimation procedures. In *Fracture Toughness, Proc.* 1971 *Nat. Symp. Fract. Mech.* (Edited by H. T. Corten), Part II, ASTM STP 514 pp. 40–69. American Society for Testing and Materials, PA.

Delale, F. and Erdogan, F. (1981). Line-spring model for surface cracks in a Reissner plate. *Int. J. Engng Sci.* **19,** 1331–1340.

Dodds, R. H., Jr and Read, D. T. (1990). Experimental and numerical studies of the *J*-integral for a surface flaw. *Int. J. Fract.* **43,** 27–67.

Du, Z.-Z. and Hancock, J. W. (1991). The effect of non-singular stresses on crack-tip constraint. *J. Mech. Phys. Solids* **39,** 555–567.

Ewing, D. J. F. (1968). Calculation on the bending of rigid/plastic notched bars. *J. Mech. Phys. Solids* **16,** 205–213.

Green, A. P. (1956). The plastic yielding of shallow notched bars due to bending. *J. Mech. Phys. Solids* **4,** 259–268.

Green, A. P. and Hundy, B. B. (1956). Initial plastic yielding in notch bend tests. *J. Mech. Phys. Solids* **4,** 128–144.

Gregory, J. A. and Debourgo, R. (1982). Piecewise rational quadratic interpolation to monotonic data. *IMA J. Numer. Anal.* **2,** 123–130.

Harlin, G. and Willis, J. R. (1988). The influence of crack size on the ductile–brittle transition. *Proc. R. Soc. London* **A415,** 197–226.

Hauf, D. E., Parks, D. M. and Lee, H. (1994). A modified effective crack-length formulation in elastic–plastic fracture mechanics. *Mech. Mater.* (in press).

Irwin, G. R. (1958). Fracture. In *Handbuch der Physik VI* (Edited by S. Flugge), pp. 551–590. Springer, Berlin.

Kim, Y.-J., McClintock, F. A. and Parks, D. M. (1994a). Yield locus in deep, single-face-cracked specimens under combined bending and tension. *J. Appl. Mech.* (in press).

Kim, Y.-J., McClintock, F. A. and Parks, D. M. (1994b). Global equilibrium of the least upper bound circular arcs and its application to fracture mechanics. Submitted to *Mech. Mater.*

Kumar, V. and German, M. D. (1985). Studies of the line-spring model for nonlinear crack problems. *J. Press. Vessel Tech.* **107,** 412–420.

Larsson, S. G. and Carlsson, A. J. (1973). Influence of non-singular stress terms and specimen geometry on small-scale yielding at crack tips in elastic–plastic material. *J. Mech. Phys. Solids* **21,** 263–277.

Lee, H. and Parks, D. M. (1993). Fully plastic analyses of plane strain single-edge cracked specimens subject to combined tension and bending. *Int. J. Fract.* **63,** 329–349.

Lee, H. and Parks, D. M. (1994). Line-spring finite element for fully plastic crack growth (in preparation).

Li, F. Z., Shih, C. F. and Needleman, A. (1985). A comparison of methods for calculating energy release rate. *Engng Fract. Mech.* **21,** 405–421.

Matsoukas, G., Cotterell, B. and Mai, Y.-W. (1986). Hydrostatic stress and crack opening displacement in three-point bend specimens with shallow cracks. *J. Mech. Phys. Solids* **34,** 499–510.

McMeeking, R. M. (1977). Finite deformation analysis of crack-tip opening in elastic–plastic materials and implications for fracture. *J. Mech. Phys. Solids* **25,** 357–381.

Miyoshi, T., Shiratori, M. and Yoshida, Y. (1986). Analysis of *J*-integral and crack growth for surface cracks by line spring method. *J. Press. Vessel Tech.* **108,** 305–311.

Nakamura, T. and Parks, D. M. (1992). Determination of elastic *T*-stress along three-dimensional crack fronts using an interaction integral. *Int. J. Solids Structures* **29,** 1579–1611.

O'Dowd, N. P. and Shih, C. F. (1991). Family of crack-tip fields characterized by a triaxiality parameter. Part I—Structure of fields. *J. Mech. Phys. Solids* **39,** 989–1015.

O'Dowd, N. P. and Shih, C. F. (1992). Family of crack-tip fields characterized by a triaxiality parameter. Part II—Fracture applications. *J. Mech. Phys. Solids* **40,** 939–963.

Parks, D. M. (1977). The virtual crack extension method for nonlinear material behavior. *Comp. Meth. Appl. Mech. Engng* **12,** 353–364.

Parks, D. M. (1981). The inelastic line-spring: estimates of elastic–plastic fracture mechanics parameters for surface-cracked plates and shells. *J. Press. Vessel Tech.* **103,** 246–254.

Parks, D. M. (1991). Three-dimensional aspects of HRR-dominance. In *Defect Assessment in Components—Fundamentals and Applications* (Edited by J. C. Blauel and K.-H. Schwalbe), ESIS/EGF9, pp. 206–231. Mechanical Engineering Publications, London.

Parks, D. M. (1992). Advances in characterization of elastic–plastic crack-tip fields. In *Topics in Fracture and Fatigue* (Edited by A. S. Argon), pp. 58–98. Springer-Verlag, New York.

Parks, D. M. and White, C. S. (1982). Elastic–plastic line-spring finite elements for surface-cracked plates and shells. *J. Press. Vessel Tech.* **104,** 287–292.

Parks, D. M., Lockett, R. R. and Brockenbrough, J. R. (1981). Stress intensity factors for surface-cracked plates and cylindrical shells using line-spring finite elements. In *Advances in Aerospace Structures and Materials* (Edited by S. S. Wang and W. R. Renton), AD-01, pp. 279–285. American Society of Mechanical Engineers, New York.

Prager, W. (1959). *An Introduction to Plasticity.* Addison-Wesley, New York.

Rice, J. R. (1972a). The line-spring model for surface flaws. In *The Surface Crack: Physical Problems and Computational Solutions* (Edited by J. L. Swedlow), pp. 171–185. American Society of Mechanical Engineers, New York.

Rice, J. R. (1972b). Some remarks on elastic crack tip fields. *Int. J. Solids Structures* **8,** 751–758.

Rice, J. R. (1974). Limitations to the small-scale yielding approximation for crack-tip plasticity. *J. Mech. Phys. Solids* **22,** 17–26.

Rice, J. R. and Levy, N. (1972). The part-through surface crack in an elastic plate. *J. Appl. Mech.* **39,** 185–194.

Rice, J. R., Paris, P. C. and Merkle, J. G. (1973). Some further results of *J*-integral analysis and estimates. In *Progress in Flaw Growth and Fracture Toughness Testing*, ASTM STP 536, pp. 231–245. American Society for Testing and Materials, PA.

Sham, T. L. (1983). A finite-element study of the asymptotic near-tip fields for mode I plane-strain cracks growing stably in elastic–ideally plastic solids. In *Elastic–Plastic Fracture*: *2nd Symp. Vol. I—Inelastic Crack Analysis* (Edited by C. F. Shih and J. P. Gudas), ASTM STP 803, pp. I-52–I-79. American Society for Testing and Materials, PA.

Sham, T. L. (1991). The determination of the elastic T-term using higher order weight functions. *Int. J. Fract.* **48,** 81–102.

Sharma, S. M., Aravas, N. and Zelman, M. G. (1994). Two-parameter characterization of crack tip fields in edge-cracked geometries: plasticity and creep solutions. In *Fracture Mechanics*: *25th Vol.* (Edited by F. Erdogan and R. J. Hartranft), ASTM STP 1220. American Society for Testing and Materials, PA (in press).

Shawki, T. G., Nakamura, T. and Parks, D. M. (1989). Line-spring analysis of surface flawed plates and shells using deformation theory. *Int. J. Fract.* **41,** 23–38.

Shih, C. F. (1981). Relationships between the J-integral and the crack opening displacement for stationary and extending cracks. *J. Mech. Phys. Solids* **29,** 305–326.

Shiratori, M. and Miyoshi, T. (1980). Evaluation of constraint factor and J-integral for single-edge notched specimen. In *Mechanical Behavior of Materials, Proc. 3rd Int. Conf. Mater.* (Edited by K. J. Miller and R. F. Smith), Vol. 3, pp. 425–434. Cambridge, U.K.

Tada, H., Paris, P. C. and Irwin, G. R. (1985). *The Stress Analysis of Cracks Handbook*. Fracture Proof Design, Saint Louis, MO.

Tracey, D. M. (1976). Finite element solutions for crack-tip behavior in small-scale yielding. *J. Engng Mater. Tech.* **98,** 146–151.

Wang, Y.-Y. (1991). A two-parameter characterization of elastic–plastic crack tip fields and applications to cleavage fracture. Ph.D. dissertation, Department of Mechanical Engineering, Massachusetts Institute of Technology, MA.

Wang, Y.-Y. (1993). On the two-parameter characterization of elastic–plastic crack-front fields in surface-cracked plates. In *Constraint Effects in Fracture* (Edited by E. M. Hackett, K.-H. Schwalbe and R. H. Dodds, Jr), ASTM STP 1171, pp. 120–138. American Society for Testing and Materials, PA.

Wang, Y.-Y. and Parks, D. M. (1992). Evaluation of the elastic T-stress in surface-cracked plates using the line-spring method. *Int. J. Fract.* **56,** 25–40.

Wang, Y.-Y. and Parks, D. M. (1994). Limits of J–T characterization of elastic–plastic crack-tip fields. In *Constraint Effects in Fracture*: *Theory and Applications* (Edited by M. Kirk and A. Bakker), ASTM STP 1244. American Society for Testing and Materials, PA (in press).

White, C. S., Ritchie, R. O. and Parks, D. M. (1983). Ductile growth of part-through surface cracks: experiment and analysis. In *Elastic–Plastic Fracture*: *2nd Symp. Vol. I—Inelastic Crack Analysis* (Edited by C. F. Shih and J. P. Gudas), ASTM STP 803, pp. I-384–I-409. American Society for Testing and Materials, PA.

Williams, M. L. (1957). On the stress distribution at the base of a stationary crack. *J. Appl. Mech.* **24,** 111–114.

APPENDIX

To be used for revising the estimates of nodal forces or displacements in a global model composed of shell and line-spring finite elements, the following Jacobian matrices are found and sent to the main body of the ABAQUS finite element program, in which global equilibrium equations are solved by Newton-type iterative methods (ABAQUS, 1988a).

A1. *Elastic Jacobian matrix* $T_{ij}^{(e)}$

We can find $\partial q_i/\partial Q_j$ from eqn (12); then the elastic Jacobian matrix $T_{ij}^{(e)} \equiv \partial Q_i/\partial q_j = [\partial q_i/\partial Q_j]^{-1}$ is given by

$$T_{ij}^{(e)} = \left[\frac{2}{H}\int_0^a \left(\frac{\partial K_I}{\partial Q_i}\frac{\partial K_I}{\partial Q_j} + K_I\frac{\partial^2 K_I}{\partial Q_i \partial Q_j}\right)\mathrm{d}\bar{a}\right]^{-1}. \tag{A1}$$

The partial derivatives in eqn (A1) are obtained by making use of eqn (7) as

$$\frac{\partial K_I}{\partial Q_i} = F_i(a_{\mathrm{eff}}, t) + F_k'(a_{\mathrm{eff}}, t)\, Q_k \frac{\partial a_{\mathrm{eff}}}{\partial Q_i} \tag{A2}$$

$$\frac{\partial^2 K_I}{\partial Q_i \partial Q_j} = F_i'(a_{\mathrm{eff}}, t)\frac{\partial a_{\mathrm{eff}}}{\partial Q_j} + F_k''(a_{\mathrm{eff}}, t)Q_k\frac{\partial a_{\mathrm{eff}}}{\partial Q_i}\frac{\partial a_{\mathrm{eff}}}{\partial Q_j} + F_j'(a_{\mathrm{eff}}, t)\frac{\partial a_{\mathrm{eff}}}{\partial Q_i} + F_k'(a_{\mathrm{eff}}, t)Q_k\frac{\partial^2 a_{\mathrm{eff}}}{\partial Q_i \partial Q_j} \tag{A3}$$

where the prime denotes differentiation with respect to a_{eff} or $\hat{a}_{\mathrm{eff}}$, depending on the argument in the parentheses. From eqn (4), the partial derivative of effective crack length with respect to the generalized force is given by

$$\frac{\partial a_{\mathrm{eff}}}{\partial Q_i} = \eta_1 t_i(a_{\mathrm{eff}}, t) + \eta_2\left[F_i(\hat{a}_{\mathrm{eff}}, t) + F_k'(\hat{a}_{\mathrm{eff}}, t)\, Q_k\frac{\partial \hat{a}_{\mathrm{eff}}}{\partial Q_i}\right] \tag{A4}$$

where

$$\eta_1 = \frac{\beta\,(\partial\rho/\partial\tau)\,K_I^2\,(\hat{a}_{\text{eff}}, t)/\sigma_y^3}{1-\beta\,(\partial\rho/\partial\tau)\,\tau'\,(a_{\text{eff}}, t)\,K_I^2\,(\hat{a}_{\text{eff}}, t)/\sigma_y^2}$$

$$\eta_2 = \frac{2\beta\,\rho\,(\tau)\,K_I\,(\hat{a}_{\text{eff}}, t)/\sigma_y^2}{1-\beta\,(\partial\rho/\partial\tau)\,\tau'\,(a_{\text{eff}}, t)\,K_I^2\,(\hat{a}_{\text{eff}}, t)/\sigma_y^2}$$

and also, from eqn (6),

$$\frac{\partial\hat{a}_{\text{eff}}}{\partial Q_i} = \frac{0.3\beta\,K_I\,(\hat{a}_{\text{eff}}, t)\,F_i\,(\hat{a}_{\text{eff}}, t)/\sigma_y^2}{1-0.3\beta\,K_I\,(\hat{a}_{\text{eff}}, t)\,F_k'\,(\hat{a}_{\text{eff}}, t)\,Q_k/\sigma_y^2}. \tag{A5}$$

The complementary energy formulation in (12) provides a symmetric Jacobian matrix (A1). Shawki *et al.* (1989) took an effective crack length into account in the elastic part of their deformation plasticity line-spring model for moderately deep cracks. Adopting the value of $K_I = F_i(a, t)Q_i$ in the correction part, they obtained an asymmetric elastic tangent tensor and neglected the slight asymmetry in computation. Here, we note that a simple secant compliance formulation such as $q_i = P_{ij}(a_{\text{eff}}, t)\,Q_j$ fails to provide a symmetric Jacobian matrix, even if $K_I = F_i(a_{\text{eff}}, t)\,Q_i$ is used in the correction part of effective crack length, owing to the dependence of a_{eff} on T as well as K_I.

A2. *Elastic–plastic Jacobian matrix* $T_{ij}^{(ep)}$

When elastic–plastic constitutive equations (18)–(20) and (24) of the line-spring element are satisfied at the end of time increment, we can derive the elastic–plastic Jacobian $T_{ij}^{(ep)}$.

We may rewrite the normality condition (17) as $\Delta q_i^{(p)} = \Lambda\Phi_{,i} = \Delta\varepsilon_o^{(p)} m\Phi_{,i} \equiv \Delta\varepsilon_o^{(p)} n_i$, where $m = f\sigma_o l^2/(Q_i\Phi_{,i})$ from eqn (24), and $n_i \equiv m\Phi_{,i}$. Then, taking the total differential of eqn (18) and rearranging leads to

$$[\delta_{ik} + \Delta\varepsilon_o^{(p)}\,S_{ij}n_{j,k}]\,\mathrm{d}(\Delta Q_k) = S_{ij}\,\mathrm{d}(\Delta q_j) - \kappa S_{ij}n_j\,\mathrm{d}(\Delta\varepsilon_o^{(p)}), \tag{A6}$$

where $n_{j,k} \equiv \partial n_j/\partial Q_k$, δ_{ik} is the Kronecker delta, and $\kappa = 1 + h_s\Delta\varepsilon_o^{(p)}/\sigma_o$. At the end of the time increment, the corrections of the solutions $\mathrm{d}(\Delta Q_i)$ and $\mathrm{d}(\Delta\varepsilon_o^{(p)})$ should also satisfy the consistency condition (19); that is,

$$\mathrm{d}\Phi = \Phi_{,i}\,\mathrm{d}(\Delta Q_i) + \frac{\partial\Phi}{\partial\sigma_o}\frac{\partial\sigma_o}{\partial\varepsilon_o^{(p)}}\mathrm{d}(\Delta\varepsilon_o^{(p)}) = 0. \tag{A7}$$

Multiplying (A7) by m and using eqn (20) gives

$$n_i\,\mathrm{d}(\Delta Q_i) + mh_s\frac{\partial\Phi}{\partial\sigma_o}\mathrm{d}(\Delta\varepsilon_o^{(p)}) = 0. \tag{A8}$$

Taking the scalar product of n_i with (A6) and introducing (A8) into the result provides

$$-mh_s\frac{\partial\Phi}{\partial\sigma_o}\mathrm{d}(\Delta\varepsilon_o^{(p)}) + \Delta\varepsilon_o^{(p)}n_iS_{ij}n_{j,k}\,\mathrm{d}(\Delta Q_k) = n_iS_{ij}\,\mathrm{d}(\Delta q_j) - \kappa n_iS_{ij}n_j\,\mathrm{d}(\Delta\varepsilon_o^{(p)})$$

which can be rewritten as

$$\mathrm{d}(\Delta\varepsilon_o^{(p)}) = \frac{1}{D}[n_iS_{ij}\,\mathrm{d}(\Delta q_j) - \Delta\varepsilon_o^{(p)}\,n_iS_{ij}\,n_{j,k}\,\mathrm{d}(\Delta Q_k)] \tag{A9}$$

where

$$D = \kappa n_{ni}S_{mn}n_n - mh_s\frac{\partial\Phi}{\partial\sigma_o}.$$

Inserting (A9) back into eqn (A6) and rearranging terms provides

$$N_{ik}\,\mathrm{d}(\Delta Q_k) = \left[S_{ij} - \frac{\kappa}{D}S_{im}n_mn_nS_{nj}\right]\mathrm{d}(\Delta q_j), \tag{A10}$$

where

$$N_{ik} = \delta_{ik} + \Delta\varepsilon_o^{(p)}\left(S_{ij} - \frac{\kappa}{D}S_{im}n_mn_nS_{nj}\right)n_{j,k}.$$

Premultiplying (A10) by N_{ik}^{-1}, we obtain the elastic–plastic Jacobian matrix $T_{ij}^{(ep)}$ as

$$T_{ij}^{(ep)} \equiv \frac{\partial Q_i}{\partial q_j} = N_{ik}^{-1}\left[S_{kj} - \frac{\kappa}{D} S_{km} n_m n_n S_{nj}\right]. \tag{A11}$$

The Jacobian matrices are used only for revising the estimated displacement fields and have no effect on the accuracy of the solution to global equilibrium equations. Instead, the accuracy of the solution at each increment is affected by the value of the prescribed tolerance of force and moment, and integration operator (ABAQUS, 1988a).